QED & QCD CORRECTIONS AT HERA

JB, OCT 7. 93

GRANADA, SPAIN

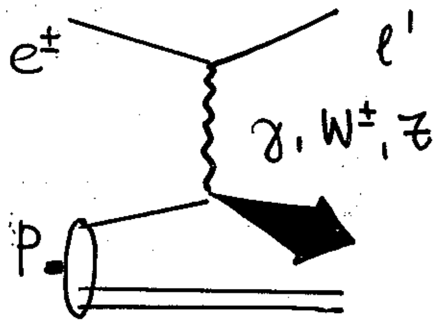

- CORRECTIONS (QED, QCD) HAVE TO BE KNOWN TO EXTRACT THE BORN CROSS SECTIONS
  - → INCLUSIVE $\sigma_{nc}^{\pm}, \sigma_{cc}^{\pm}$
  - → EXCLUSIVE $Z', \phi_{LQ}^{S,V}$, ✗, $e^{\pm}p \to W^{\pm}(Z)X$ etc.

  ⟶ THE CORRECTIONS TURN OUT TO BE LARGE IN SOME RANGES

- ONE MAY EXTRACT INFORMATION FROM THE RC'S THEMSELVES.
  - → QCD: Λ, $xG(x, Q^2)$
  - → QED: 'COMPTON' SUBSET : $F_{2,L}$ $Q^2 \ll M_p^2$, $x \ll 1$ (NONPERTURBATIVE)

- NOVEL QCD DYNAMICS AT SMALL x.

$$P_{ff}(x) = \delta(1-x) + \frac{\alpha e_f^2}{2\pi}\log\left(\frac{Q^2}{m_f^2}\right)\left\{\frac{1+x^2}{1-x} + \frac{3}{2}\delta(1-x)\right\} + \mathcal{O}(\alpha^2)$$

Due to the Weierstrass' polynomial theorem and the conservation of probability one has

$$\int_0^1 dx P_{ff}^{(0)}(x) = 1 \quad \text{and} \quad \int_0^1 dx P_{ff}^{(1)}(x) = 0$$

where (n) denotes the order in α.

$\mathcal{O}(\alpha)$:
QED.

LLA.

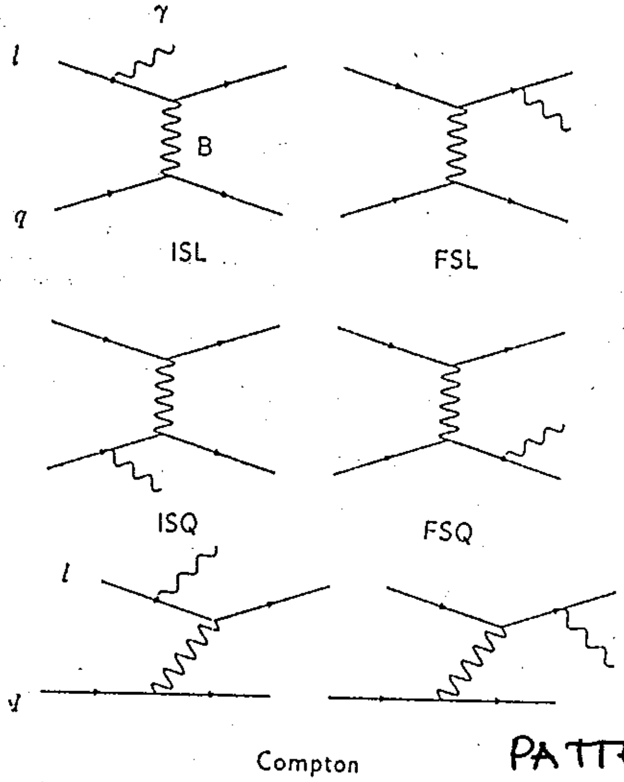

PATTERN KNOWN FROM QCD ANOM. DIM

$\mathcal{O}(\alpha^2_{LO})$ $\mathcal{O}(\alpha^2)$ Non lead.

$\mathcal{O}(\alpha^3)_{LO}$.

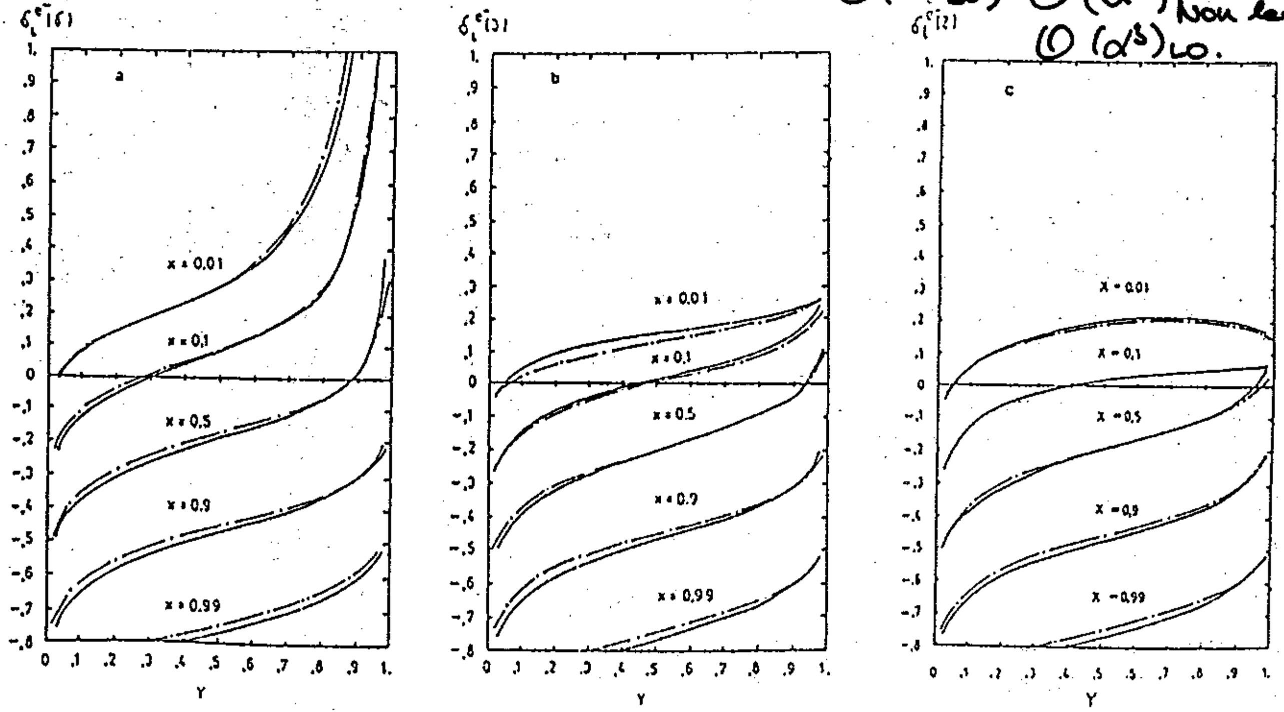

Figure 11: Relative LLA QED corrections in $\mathcal{O}(\alpha)$ for the photon exchange term (a), $\gamma - Z$ interference term (b), and the Z exchange term for neutral current deep inelastic scattering at $\sqrt{s} = 314$ GeV (full lines) (c). For comparison the result of a [illegible] calculation [15] is shown (dash-dotted lines); from [17].

EXPON: NS - evolution equations.

OTHER VARIABLES

Due to the finite resolution of the electromagnetic calorimeter measuring the electromagnetic (e', γ) final state it may be difficult to resolve the final state photon from the electron in practice. According to the Kinoshita–Lee–Nauenberg (KLN) theorem [24] the fsr term vanishes in this case.

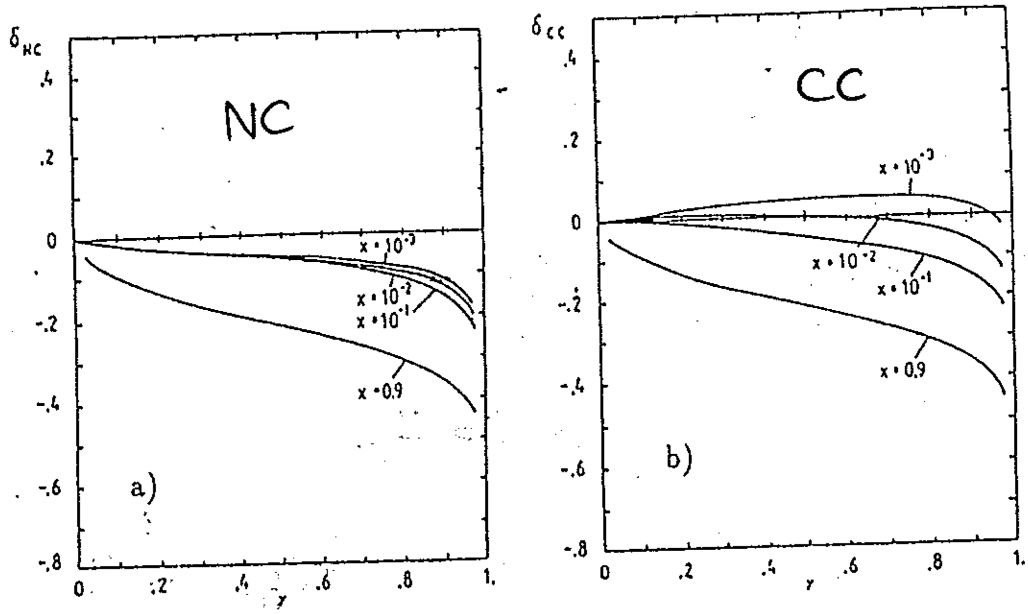

JET MEAS.

Figure 12: $\mathcal{O}(\alpha)$ leading log QED corrections to deep inelastic scattering using jet measurement at $\sqrt{s} = 314$ GeV in dependence of x and y. a) neutral current scattering; b) charged current scattering, [20].

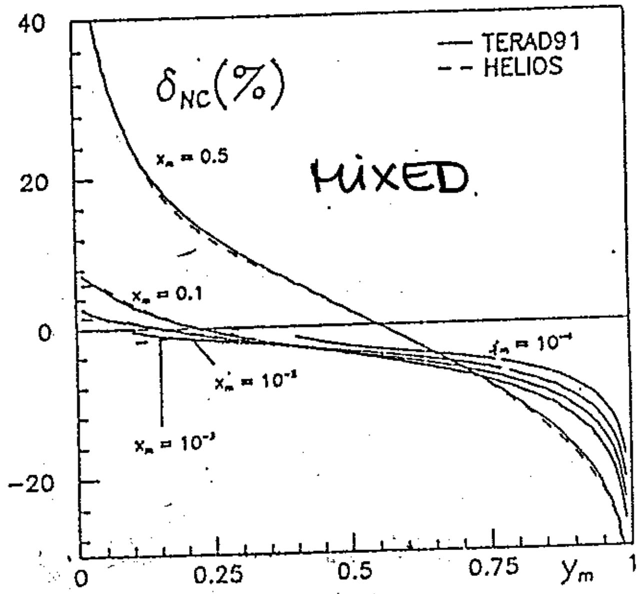

Figure 13: QED leptonic corrections to $d\sigma/dxdy$ for mixed variables in per cent. Full lines are complete $\mathcal{O}(\alpha)$ results from TERAD91 [25], the dashed lines represent results from the leading logarithmic approximation (see [20]) obtained from HELIOS [23]; from [13].

- HIGHER ORDERS & STABILITY

⟶ CORERS IN PHASE SPACE.

'COMPTON' PROCESS

JB, LEVMAN, SPIESBERGER

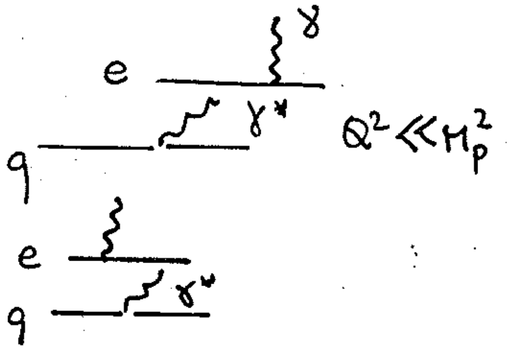

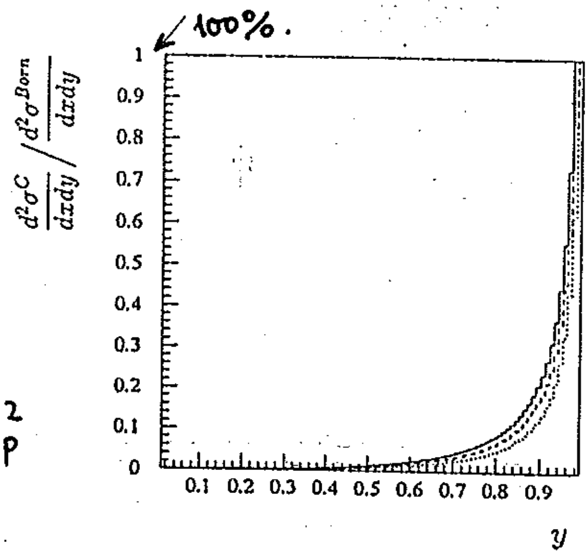

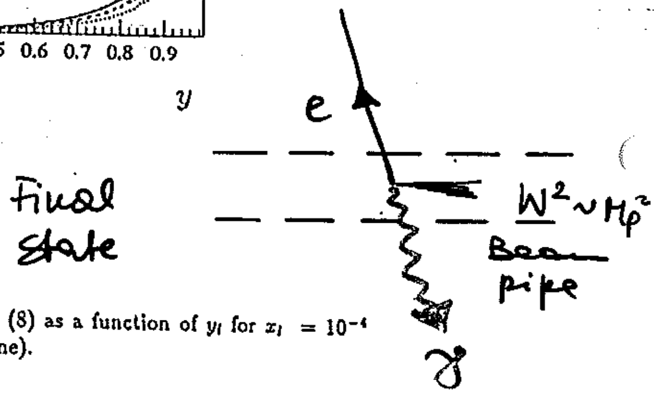

Figure 1: Differential Compton cross section Eq. (8) as a function of y_l for $x_l = 10^{-4}$ (dotted line), 10^{-3} (dashed line), and 10^{-2} (full line).

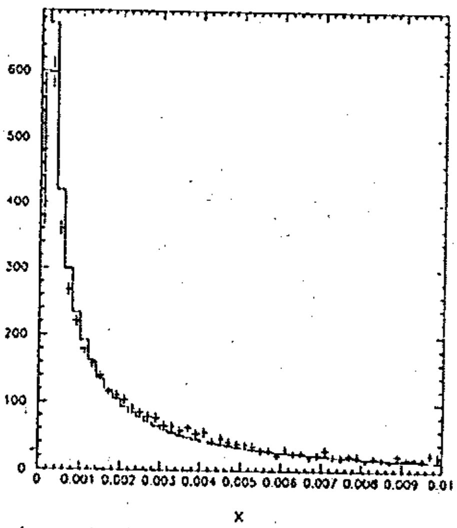

Figure 5: The expected photon density after the extraction procedure described in the text. The errors represent the statistical errors for an integrated luminosity of 100 pb^{-1}. The solid histogram is the prediction of Eq. (13) for HMRSB [21]. The units of the vertical scale are arbitrary.

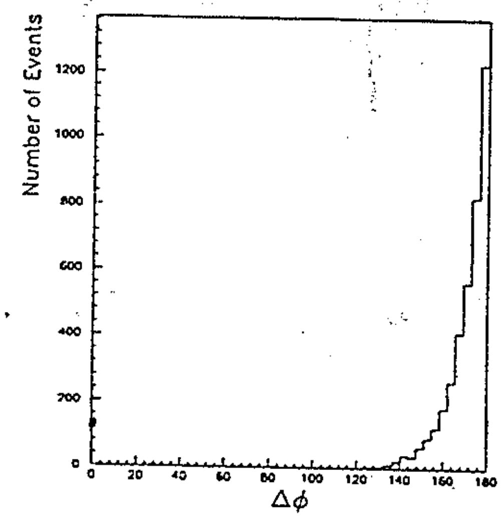

Figure 2: The difference in azimuth of the photon and electron for accepted Compton events.

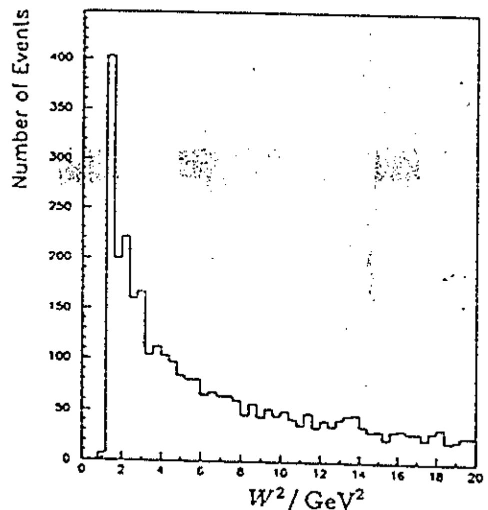

Figure 3: The hadronic mass distribution W^2 for accepted Compton events.

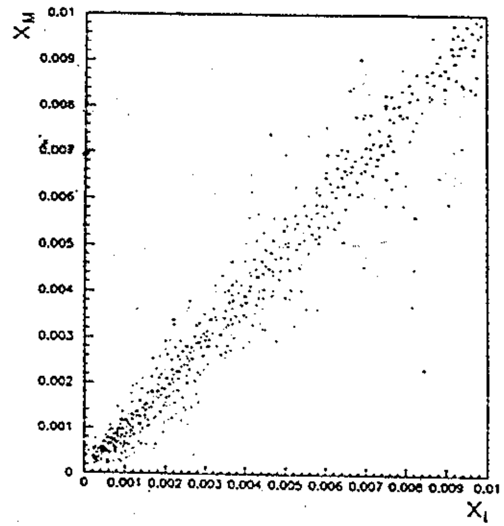

Figure 4: A scatter plot of $x_l = Q_l^2/2p\cdot(l-l')$ and $x_M = M_{e\gamma}^2/s$.

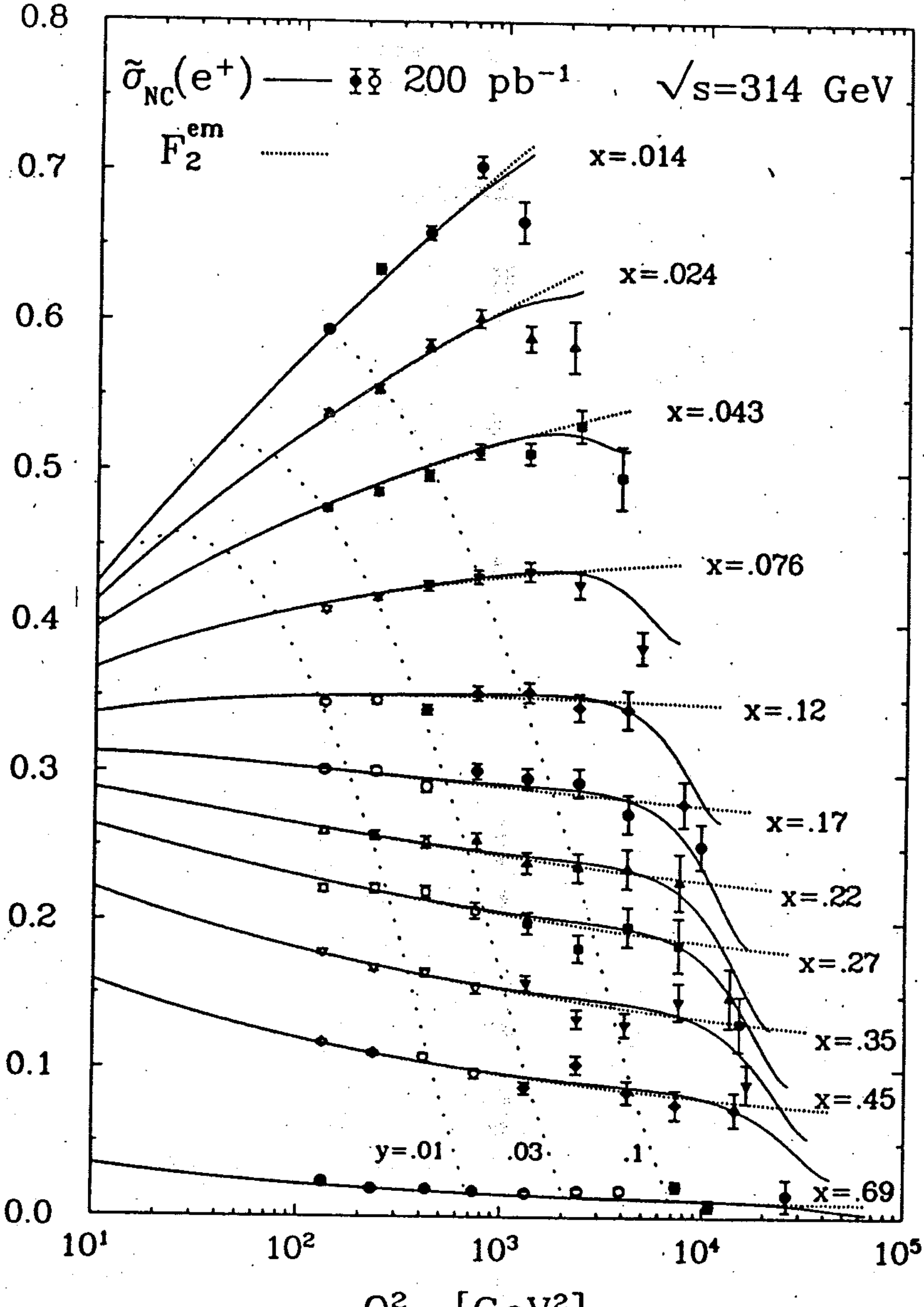

σ̃NC(e+) —— 200 pb-1
√s=314 GeV
F2em ········
x=.014
x=.024
x=.043
x=.076
x=.12
x=.17
x=.22
x=.27
x=.35
x=.45
x=.69
y=.01
.03
.1
0.8
0.7
0.6
0.5
0.4
0.3
0.2
0.1
0.0
10^1
10^2
10^3
10^4
10^5
Q^2 [GeV^2]

Fig. 3

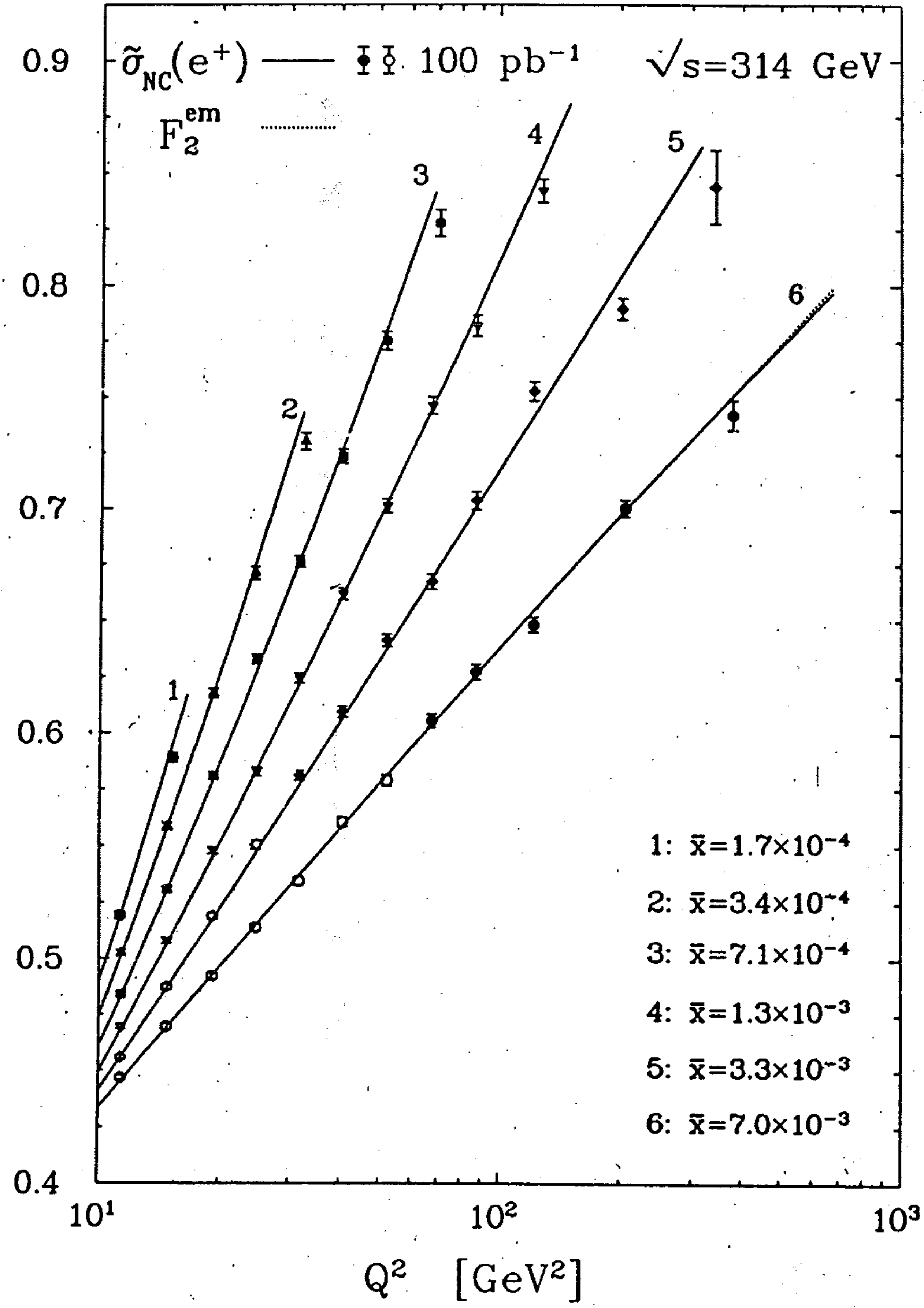

$\tilde{\sigma}_{NC}(e^+)$ — ⧫ ⧫ 100 pb^{-1}
$\sqrt{s}$=314 GeV
F_2^{em}
0.9
0.8
0.7
0.6
0.5
0.4
1
2
3
4
5
6
1: $\bar{x}=1.7\times10^{-4}$
2: $\bar{x}=3.4\times10^{-4}$
3: $\bar{x}=7.1\times10^{-4}$
4: $\bar{x}=1.3\times10^{-3}$
5: $\bar{x}=3.3\times10^{-3}$
6: $\bar{x}=7.0\times10^{-3}$
10^1
10^2
10^3
Q^2 [GeV^2]

Fig. 6

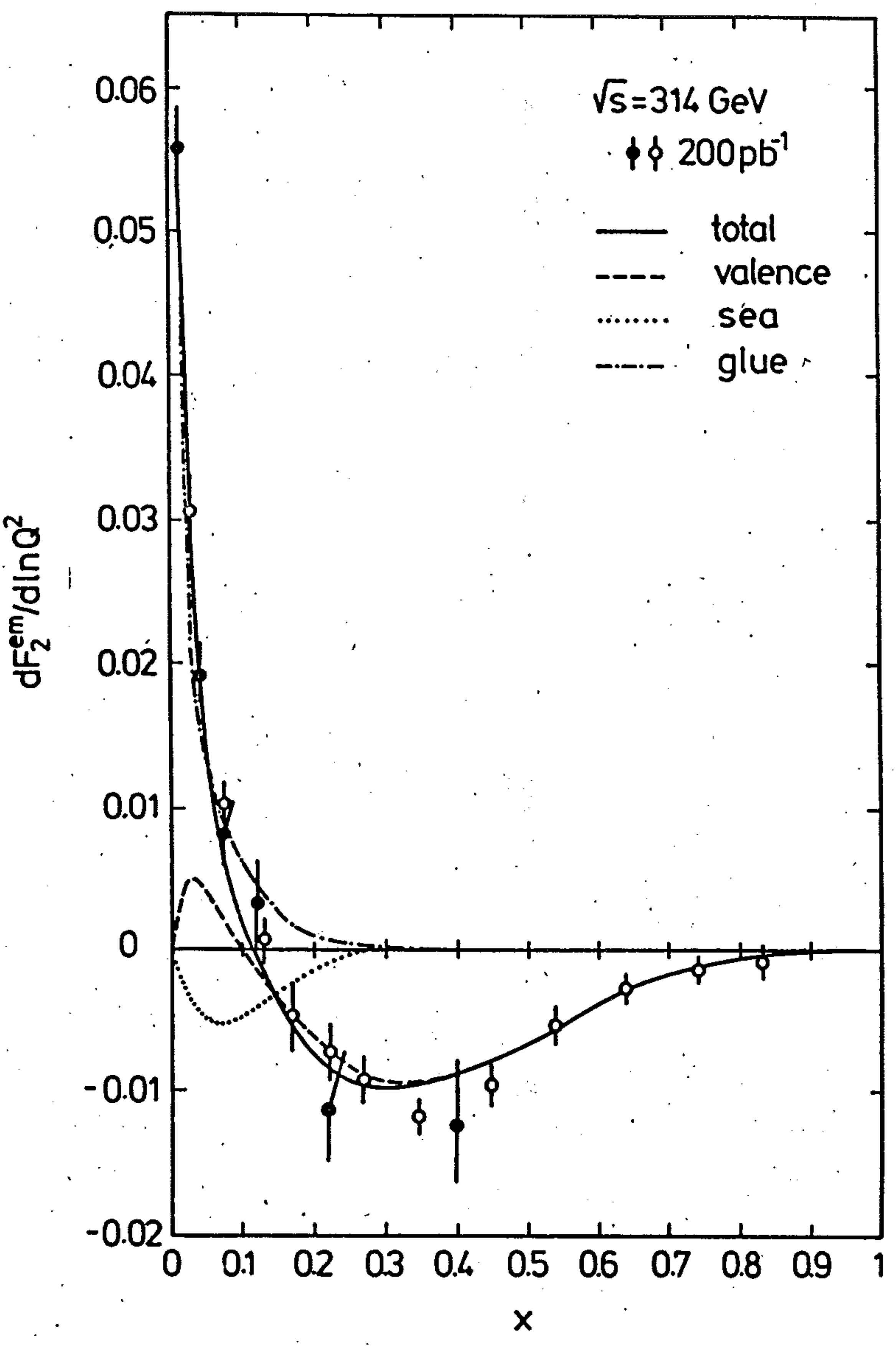
$\sqrt{s}$=314 GeV
200 pb^{-1}
total
valence
sea
glue
$dF_2^{em}/d\ln Q^2$
0.06
0.05
0.04
0.03
0.02
0.01
0
-0.01
-0.02
0
0.1
0.2
0.3
0.4
0.5
0.6
0.7
0.8
0.9
1
x

Fig.5

QCD CORRECTIONS & QCD TESTS

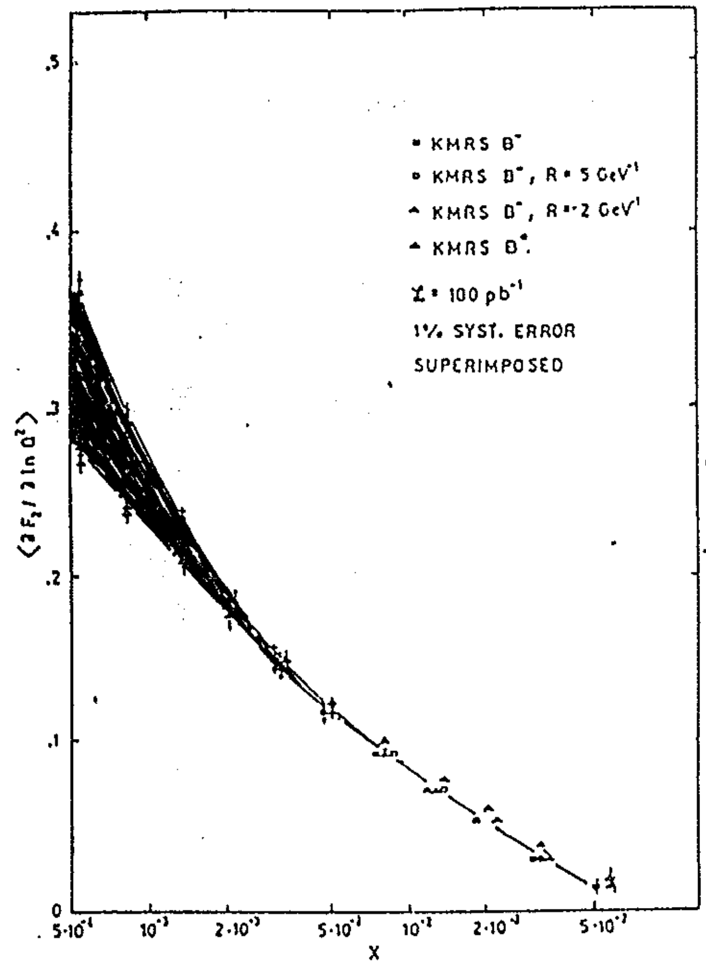

SCREENING CORRECTIONS:
'NON LIN.' DYN.
→ HIGHER TWISTS

SOL. OF AP. EQUATIONS: ⟹ Λ_{QCD}

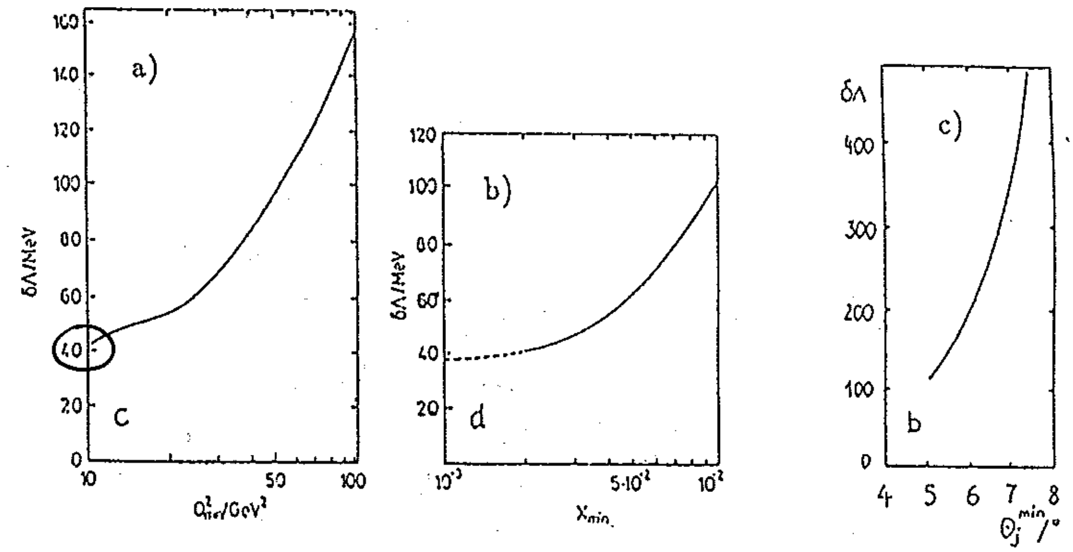

Figure 43: Dependence of $\delta\Lambda_{stat}$ on the minimum Q^2 (a) and x (b) used in the QCD fit for the combined data sets at $\sqrt{s}$ = 110 and 314 GeV for $\mathcal{L}$ = $100pb^{-1}$ each; (c) dependence of $\delta\Lambda_{stat}$ for $x \geq 0.25$, $\mathcal{L} = 100pb^{-1}$, $\sqrt{s} = 110$ GeV on the minimum jet angle; [34].

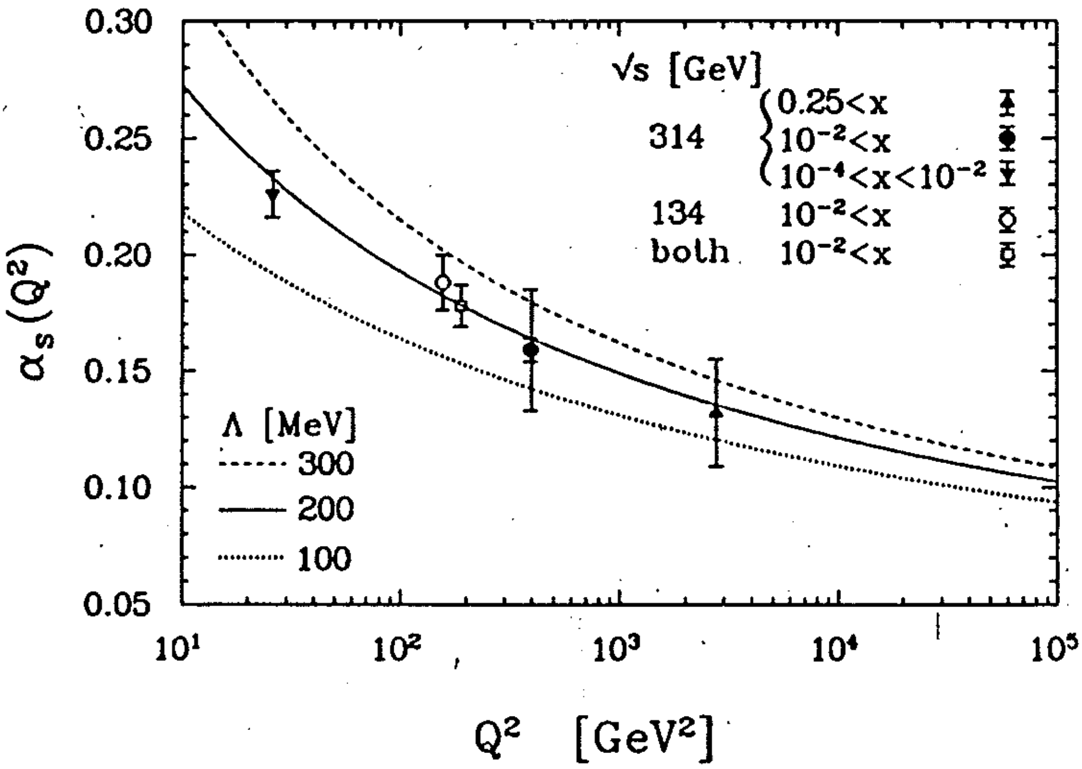
0.30
0.25
0.20
0.15
0.10
0.05
$\alpha_s(Q^2)$
$\sqrt{s}$ [GeV]
314
0.25<x
10^{-2}<x
10^{-4}<x<10^{-2}
134 10^{-2}<x
both 10^{-2}<x
Λ [MeV]
300
200
100
10^1
10^2
10^3
10^4
10^5
Q^2 [GeV^2]

Fig. 8

$F_L(x, Q^2)$ & $xG(x, Q^2)$

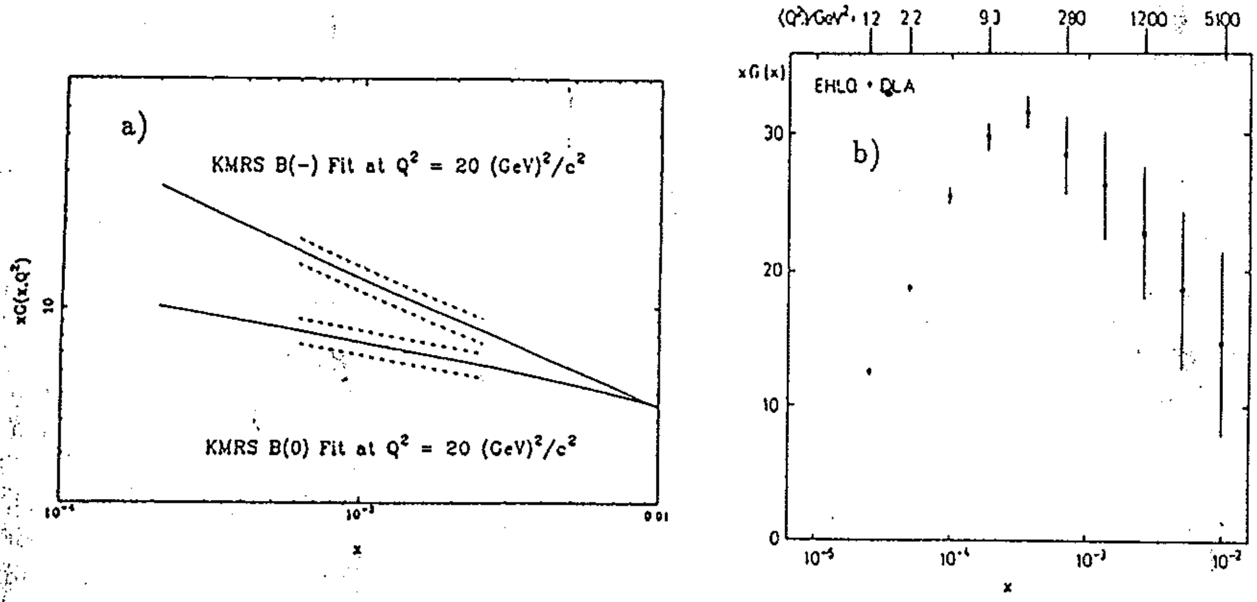

Figure 33: (a) Gluon distribution at low x and measureable domain with errors at HERA, [57]; (b) statistical precision of a possible measurement of $xG(x)$ at LEP ⊗ LHC using (62). Here, F_L was determined in the overlap range of a combined measurement at $\sqrt{s} = 1265$ GeV, $\mathcal{L} = 1 fb^{-1}$, and $\sqrt{s} = 1789$ GeV, $\mathcal{L} = 100 pb^{-1}$, and the average over Q^2 was taken, from [36].

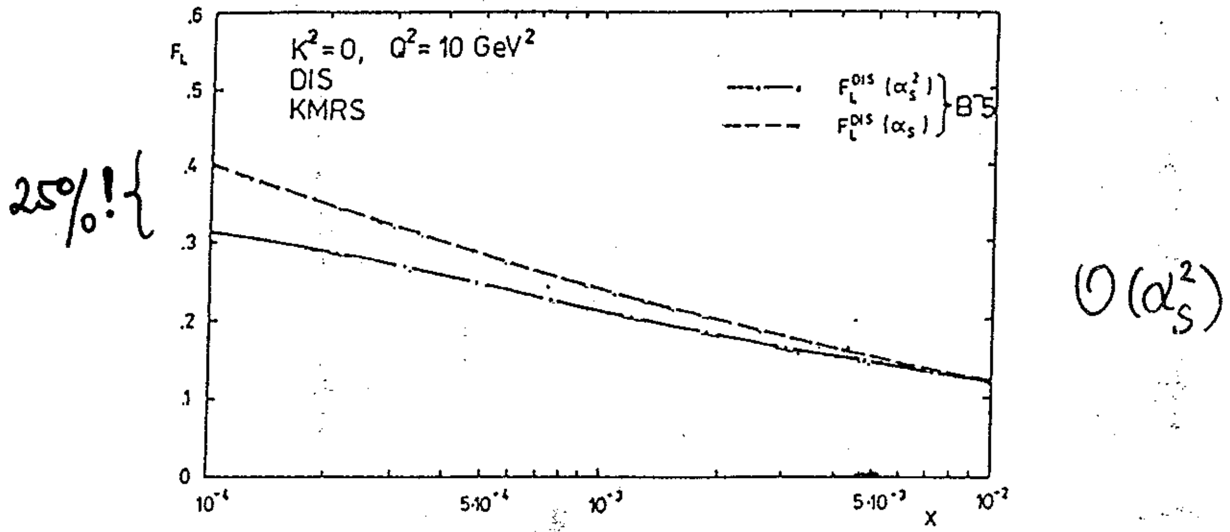

Figure 34: Comparison of 1st and 2nd order contributions to $F_L(x, Q^2)$ [59] for $Q^2 = 10\,\mathrm{GeV}^2$ using the parton distributions KMRS B^- [32].

$$\frac{d^2\sigma}{dQ^2dy} = 2\pi\alpha^2\frac{Ms}{(s-M^2)^2}\frac{1}{Q^4}L_{\mu\nu}W^{\mu\nu} \tag{5}$$

For only electromagnetic interactions[4] the leptonic and hadronic tensor $L_{\mu\nu}$ and $W_{\mu\nu}$ are given by

$$\begin{aligned} L_{\mu\nu} &= 2\left[l_\mu l'_\nu + l'_\mu l_\nu - g_{\mu\nu} l.l'\right] \\ W_{\mu\nu} &= \left(-g_{\mu\nu} + \frac{q_\mu q_\nu}{q^2}\right) W_1(x,Q^2) + \frac{1}{M^2}\left[\left(P_\mu - \frac{P.q}{q^2}q_\mu\right)\left(P_\nu - \frac{P.q}{q^2}q_\nu\right)\right] W_2(x,Q^2) \end{aligned} \tag{6}$$

with l and l' the incoming and outgoing lepton 4–momenta, and M the proton mass. In the Bjorken–limit the longitudinal structure function $F_L(x,Q^2)$ is obtained via the projection

$$\frac{P.q}{M^2}W_2(x,Q^2) - 2xW_1(x,Q^2) \to F_L(x,Q^2) = \frac{8x^3}{Q^2}P_\mu P_\nu W^{\mu\nu} \tag{7}$$

The dominant contribution to $F_L(x,Q^2)$ is obtained from the gluon contribution. The corresponding coefficient function is given by

$$\begin{aligned} f_L^{qG}(K^2,x,Q^2) &= \frac{\alpha_s e_q^2}{4\pi}\left\{\frac{4Q^4}{K^4 x}G_{1L}(\beta,\zeta) + \frac{xQ^2}{K^2}\frac{1}{\sqrt{1-\zeta}}\log\left|\frac{1+\sqrt{1-\zeta}}{1-\sqrt{1-\zeta}}\right| G_{2L}(\beta,\zeta)\right. \\ &\quad \left. + \frac{2xQ^2}{K^2}G_{3L}(\beta,\zeta)\right\} \end{aligned} \tag{8}$$

where

$$\zeta = \frac{4K^2x^2}{Q^2} \qquad \cos\beta = \frac{1-\zeta/2}{\sqrt{1-x\zeta}}$$

and β denotes the angle between gluon and proton in the virtual photon–virtual gluon cms. functions $G_{iL}(\beta,\zeta)$ in (8) may be expressed in a polynomial form by

$$G_{iL}(\beta,\zeta) = -\sum_{j=0}^{4} g_{ji}^{L}(\beta)\left(\frac{\zeta}{W(\zeta)}\right)^j$$

where

$$W(\zeta) = 1 - \zeta + \sqrt{1-\zeta}$$

Finally, the coefficients $g_{ji}^{(L)}$ in (10) are:

$$\begin{aligned}
g_{01}^{(L)}(\beta) &= -\frac{1}{8} + \frac{1}{4}\cos\beta - \frac{1}{4}\cos^3\beta + \frac{1}{8}\cos^4\beta \\
g_{02}^{(L)}(\beta) &= -\frac{1}{4} + 2\cos\beta - \cos^2\beta - 3\cos^3\beta + \frac{9}{4}\cos^4\beta \\
g_{03}^{(L)}(\beta) &= -\frac{1}{4} + 6\cos\beta - \frac{9}{2}\cos^2\beta - 10\cos^3\beta + \frac{35}{4}\cos^4\beta \\
g_{11}^{(L)}(\beta) &= \cos\beta - \frac{3}{4}\cos^2\beta - \frac{3}{2}\cos^3\beta + \frac{5}{4}\cos^4\beta \\
g_{12}^{(L)}(\beta) &= \frac{1}{4} + \frac{13}{2}\cos\beta - \frac{15}{2}\cos^2\beta - \frac{21}{2}\cos^3\beta + \frac{45}{4}\cos^4\beta \\
g_{13}^{(L)}(\beta) &= 1 + 18\cos\beta - 24\cos^2\beta - 30\cos^3\beta + 35\cos^4\beta \\
g_{21}^{(L)}(\beta) &= \frac{3}{16} + \frac{9}{8}\cos\beta - \frac{9}{4}\cos^2\beta - \frac{15}{8}\cos^3\beta + \frac{45}{16}\cos^4\beta \\
g_{22}^{(L)}(\beta) &= \frac{5}{4} + \frac{27}{4}\cos\beta - 15\cos^2\beta - \frac{45}{4}\cos^3\beta + \frac{75}{4}\cos^4\beta \\
g_{23}^{(L)}(\beta) &= \frac{7}{2} + 18\cos\beta - 42\cos^2\beta - 30\cos^3\beta + \frac{105}{2}\cos^4\beta \\
g_{31}^{(L)}(\beta) &= \frac{3}{16} + \frac{6}{16}\cos\beta - \frac{15}{8}\cos^2\beta - \frac{5}{2}\cos^3\beta + \frac{35}{4}\cos^4\beta \\
g_{32}^{(L)}(\beta) &= \frac{9}{8} + \frac{9}{4}\cos\beta - \frac{45}{4}\cos^2\beta - \frac{15}{4}\cos^3\beta + \frac{105}{8}\cos^4\beta \\
g_{33}^{(L)}(\beta) &= 3 + 6\cos\beta - 30\cos^2\beta - 10\cos^3\beta + 35\cos^4\beta \\
g_{41}^{(L)}(\beta) &= \frac{3}{64} - \frac{15}{32}\cos^2\beta + \frac{35}{64}\cos^4\beta \\
g_{42}^{(L)}(\beta) &= \frac{9}{32} - \frac{45}{16}\cos^2\beta + \frac{105}{32}\cos^4\beta \\
g_{43}^{(L)}(\beta) &= \frac{3}{4} - \frac{15}{2}\cos^2\beta + \frac{35}{4}\cos^4\beta
\end{aligned}$$

The structure function $F_L(x,Q^2)$ is then given by (4) for $i = L$.

In the limit $K^2 \to 0$ the coefficient function $f_L^{qG}(x,Q^2)$ simplifies considerably and one ol the well–known result [10]

$$f_L^{qG(0)}(x,Q^2) = \frac{2}{\pi}e_q^2\alpha_s x^2(1-x)$$

$$F_{L(0)}(x,Q^2) = \sum_q \int_x^1 \frac{dz}{z} f_{2,L}^{qG}\left(\frac{x}{z}\right) zG(z,Q^2)$$

$$F_i(x,Q^2) = \sum_q \left\{ \int_x^1 \frac{d\eta}{\eta} f_i^{qG}\left(\frac{x}{\eta}\right) \eta G(\eta,Q_0^2) + \int_x^1 \frac{d\eta}{\eta} \int_{Q_0^2}^{K_{max}^2} dK^2 f_i^{qG}\left(\frac{x}{\eta},\frac{K^2}{Q^2}\right) \frac{\partial \eta G(\eta,K^2)}{\partial K^2} \right\}$$